

ORIGINAL RESEARCH

Coarse-Grid Selection Using Simulated Annealing

T. U. Zaman*¹ | S. P. MacLachlan² | L. N. Olson³ | M. West⁴¹Scientific Computing Program, Memorial University of Newfoundland, NL, Canada²Department of Mathematics and Statistics, Memorial University of Newfoundland, NL, Canada³Department of Computer Science, University of Illinois at Urbana-Champaign, Illinois, USA⁴Department of Mechanical Science and Engineering, University of Illinois at Urbana-Champaign, Illinois, USA**Correspondence**

*T. U. Zaman, Scientific Computing Program, Memorial University of Newfoundland, Newfoundland and Labrador, Canada. Email: tzaman@mun.ca

Abstract

Multilevel techniques are efficient approaches for solving the large linear systems that arise from discretized partial differential equations and other problems. While geometric multigrid requires detailed knowledge about the underlying problem and its discretization, algebraic multigrid aims to be less intrusive, requiring less knowledge about the origin of the linear system. A key step in algebraic multigrid is the choice of the coarse/fine partitioning, aiming to balance the convergence of the iteration with its cost. In work by MacLachlan and Saad¹, a constrained combinatorial optimization problem is used to define the “best” coarse grid within the setting of a two-level reduction-based algebraic multigrid method and is shown to be NP-complete. Here, we develop a new coarsening algorithm based on simulated annealing to approximate solutions to this problem, which yields improved results over the greedy algorithm developed previously. We present numerical results for test problems on both structured and unstructured meshes, demonstrating the ability to exploit knowledge about the underlying grid structure if it is available.

KEYWORDS:

Algebraic Multigrid, Coarse-Grid Selection, Simulated Annealing, Combinatorial Optimization

1 | INTRODUCTION

Multigrid and other multilevel methods are well-established algorithms for the solution of large linear systems of equations that arise in many areas of computational science and engineering. Multigrid methods arise from the observation that basic iterative methods, such as the (weighted) Jacobi and Gauss-Seidel iterations, effectively eliminate only part of the error in an approximation to the solution of the problem, and that the complementary space of errors can be corrected from a coarse representation of the problem. While geometric multigrid has been shown to be highly effective for problems where a hierarchy of discrete models can be built directly, many problems benefit from the use of algebraic multigrid (AMG) techniques, where graph-based algorithms and other heuristics are used to define the multigrid hierarchy directly from the matrix of the finest-grid problem.

First introduced in the early 1980's^{2,3}, AMG is now widely used and available in standard libraries, such as hypre^{4,5}, PETSc^{6,7}, Trilinos^{8,9}, and PyAMG¹⁰. While there are many variants of AMG (as discussed below), the common features of AMG algorithms are the use of graph-based algorithms to construct a coarse grid from the given fine-grid discretization matrix (possibly with some additional information, such as geometric locations of the degrees of freedom for elasticity problems¹¹) followed by construction of an algebraic interpolation operator from the coarse grid to the fine grid. Both of these components have received significant attention in the literature, with an abundance of schemes for creating the coarse grid and for determining the entries in interpolation. In this paper, we focus on the coarse-grid correction process, adopting a combinatorial optimization viewpoint on the selection of coarse-grid points in the classical AMG setting.

One of the primary differences between so-called classical (Ruge-Stüben) AMG and (smoothed) aggregation approaches is in how the coarse grid itself is defined¹². In aggregation-based approaches, coarse grids are defined by clustering fine-grid points into aggregates (or subdomains), while, in classical AMG, a subset of the fine-grid degrees of freedom (points) is selected in order to form the coarse grid. In the original method^{3, 13}, this was accomplished using a greedy algorithm to construct a maximal independent set over the fine-grid degrees of freedom as a “first pass” at forming the coarse-grid set, which is then augmented by a “second pass” algorithm that ensures suitable interpolation can be defined from the final coarse grid. Many alternative strategies to forming the coarse grid have been proposed over the years, particularly for the parallel case, to overcome the inherent sequentiality of the original algorithm^{5, 14–17}. Other approaches, for example based on redefining the notion of strength of connection^{18–21} or use of compatible relaxation principles^{22, 23}, have also been proposed.

One class of algorithms for AMG coarsening are those based on reduction-based AMG principles, where there is a direct connection between properties of the fine-grid submatrix and the guaranteed convergence rate of the scheme^{1, 24–26}. Reduction-based multigrid methods²⁷ are a generalization of cyclic reduction²⁸, in which conditions on the coarse/fine partitioning are relaxed so that while the exact Schur complement may not be sparse, it can be accurately approximated by a sparse matrix. This notion is made rigorous by MacLachlan et al.²⁴, who propose a theoretical framework to analyse convergence based on diagonal dominance of the fine-grid submatrix (in contrast to the fine-grid submatrix being diagonal in the classical setting of cyclic reduction), and extended to Chebyshev-style relaxation schemes by Gossler and Nabben²⁶. MacLachlan and Saad^{1, 25} used this approach to guide construction of a family of greedy coarsening algorithms that aim to maximize the size of the fine-grid set subject to maintaining a fixed level of diagonal dominance in the fine-grid submatrix (and, consequently, the resulting convergence bound on the AMG method).

In this paper, we follow the theory and framework developed by MacLachlan and co-authors^{1, 24} for the selection of coarse grids in AMG algorithms, but aim to overcome some limitations of the underlying greedy coarsening algorithm¹. In particular, we develop a coarsening algorithm based on simulated annealing to partition the coarse and fine points. Numerical results show that this algorithm achieves smaller coarse grids (than the greedy approach) that satisfy the same diagonal-dominance criterion. Hence, these grids lead to moderately more efficient (two-level) algorithms, by reducing the size of the coarse-grid problem without changing the convergence bound guaranteed by the theory.

This paper is arranged as follows. In Section 2, AMG coarsening and the existing greedy coarsening algorithm for AMGr are discussed. The new coarsening algorithm based on simulated annealing is outlined in Section 3. Numerical experiments are given in Section 4, demonstrating performance of this approach on both isotropic and anisotropic problems, discretized on both structured and unstructured meshes. Concluding remarks and potential future research are discussed in Section 5.

2 | AMG COARSENING

Geometric multigrid is known to be highly effective for many problems discretized on structured meshes. However, it is naturally more difficult to make effective coarse grids (and effective coarse-grid operators) for problems discretized on unstructured meshes. AMG was developed specifically to address this, automating the formation of coarse-grid matrices without any direct mesh information. The first coarsening approach in AMG, often called classical or Ruge-Stüben (RS) coarsening, was developed by Brandt, McCormick, and Ruge^{2, 3} and later by Ruge and Stüben¹³. We summarize this approach below, primarily to allow comparison with the reduction-based AMG method^{24, 27} and the greedy coarsening approach proposed by MacLachlan and Saad¹ that is the starting point for the research reported herein.

AMG algorithms make use of a two-stage approach, where a setup phase precedes the cycling in the solve phase. Common steps in AMG setup phases include recursively choosing a coarse grid and defining intergrid transfer operators. The details of these processes depend on the specifics of the AMG algorithm under consideration, with both point-based and aggregation-based approaches to determining the coarse grid, and a variety of interpolation schemes possible for both of these.

2.1 | Classical coarsening

As in geometric multigrid, the coarse grid in AMG is selected so that errors not reduced by relaxation can be accurately approximated on coarse grids. In an effective scheme, these errors are interpolated accurately from coarse grids that have substantially fewer degrees of freedom than the next finer grid, thus significantly reducing the cost of solving the coarse-grid residual problem.

In classical AMG, for an $n \times n$ matrix A , the index set $\Omega = \{1, \dots, n\}$ is split into sets C and F , with $\Omega = C \cup F$ and $C \cap F = \emptyset$. Each degree of freedom (DoF) or point $i \in C$ is denoted a C -point and a point $j \in F$ is denoted an F -point. This splitting is constructed by considering the so-called *strong* connections in the graph of matrix between the fine-level variables. Given a threshold value, $0 < \theta \leq 1$, the variable u_j is said to strongly influence u_i if $-A_{ij} \geq \theta \max_{k \neq i} \{-A_{ik}\}$, where A_{ij} is the coefficient of u_j in the i th equation. The set of points that strongly influence i , denoted by S_i , is defined as the set of points on which point i strongly depends. The set of points that are strongly influenced by i is denoted by S_i^T . Two heuristics are followed in RS coarsening to select a coarse grid:

H1 : For every F -point, i , every point $j \in S_i$ should either be a coarse-grid point or should strongly depend on on at least one point in C that also strongly influences i .

H2 : The set of C -points should be a maximal subset of all points, where no C -point strongly depends on another C -point.

In practice, strong enforcement of both of **H1** and **H2** is not always possible; the classical interpolation formula relies on **H1** being strongly enforced, while **H2** is used only to encourage the selection of small, sparse coarse grids.

2.2 | Greedy coarsening and underlying optimization

While the classical coarsening algorithm has proven effective for many problems when coupled with suitable construction of the interpolation operator¹³, the process provides few guarantees in practice. Indeed, there is an inherent disconnect between the selection of any single coarse-grid point and the impact on the quality of the resulting interpolation operator. This has motivated coupled approaches to selecting coarse grids and defining interpolation, including *reduction-based* AMG, or AMGr.

Reduction-based multigrid was proposed by Ries et al.²⁷, building on earlier work aiming to improve multigrid convergence for the standard finite-difference Poisson problem. The fundamental idea of reduction-based multigrid lies in defining the multigrid components to approximate those of cyclic-reduction algorithms²⁸. In particular, one way to interpret cyclic reduction is as a two-level multigrid method with idealized relaxation, interpolation, and restriction operators. Suppose that the coarse/fine partitioning is already determined, and consider the reordering of the linear system $A\mathbf{x} = \mathbf{b}$ according to the partition, writing

$$A = \begin{bmatrix} A_{FF} & -A_{FC} \\ -A_{CF} & A_{CC} \end{bmatrix} \quad \mathbf{x} = \begin{bmatrix} \mathbf{x}_F \\ \mathbf{x}_C \end{bmatrix} \quad \mathbf{b} = \begin{bmatrix} \mathbf{b}_F \\ \mathbf{b}_C \end{bmatrix}.$$

An *exact* algorithm for the solution of $A\mathbf{x} = \mathbf{b}$ in this partitioned form is given by

1. $\mathbf{y}_F = A_{FF}^{-1} \mathbf{b}_F$,
2. Solve $(A_{CC} - A_{CF} A_{FF}^{-1} A_{FC}) \mathbf{x}_C = \mathbf{b}_C + A_{CF} \mathbf{y}_F$,
3. $\mathbf{x}_F = \mathbf{y}_F + A_{FF}^{-1} A_{FC} \mathbf{x}_C$.

This can be turned into an iterative method for solving $A\mathbf{x} = \mathbf{b}$ in the usual way, by replacing the right-hand side vector, \mathbf{b} , by the evolving residual, and computing updates to a current approximation, $\mathbf{x}^{(k)}$, giving

1. $\mathbf{x}_F^{(k+1/2)} = \mathbf{x}_F^{(k)} + A_{FF}^{-1} (\mathbf{b}_F - A_{FF} \mathbf{x}_F^{(k)} + A_{FC} \mathbf{x}_C^{(k)})$,
2. Solve $(A_{CC} - A_{CF} A_{FF}^{-1} A_{FC}) \mathbf{y}_C = \mathbf{b}_C + A_{CF} \mathbf{x}_F^{(k+1/2)} - A_{CC} \mathbf{x}_C^{(k)}$,
3. $\mathbf{x}_C^{(k+1)} = \mathbf{x}_C^{(k)} + \mathbf{y}_C$,
4. $\mathbf{x}_F^{(k+1)} = \mathbf{x}_F^{(k+1/2)} + A_{FF}^{-1} A_{FC} \mathbf{y}_C$.

In this form, this remains an exact algorithm: given any initial guess, $\mathbf{x}^{(0)}$, we have the solution $\mathbf{x} = \mathbf{x}^{(1)}$. A truly iterative method results from approximating the three instances of A_{FF}^{-1} in the above algorithm, namely

$$\hat{A}_{FF}^{-1} \approx A_{FF}^{-1} \quad \hat{A}_C \approx A_{CC} - A_{CF} A_{FF}^{-1} A_{FC} \quad W_{FC} \approx A_{FF}^{-1} A_{FC}, \quad (1)$$

leading to the following iteration:

1. $\mathbf{x}_F^{(k+1/2)} = \mathbf{x}_F^{(k)} + \hat{A}_{FF}^{-1} (\mathbf{b}_F - A_{FF} \mathbf{x}_F^{(k)} + A_{FC} \mathbf{x}_C^{(k)})$,

2. Solve $\hat{A}_C \mathbf{y}_C = \mathbf{b}_C + A_{CF} \mathbf{x}_F^{(k+1/2)} - A_{CC} \mathbf{x}_C^{(k)}$,
3. $\mathbf{x}_C^{(k+1)} = \mathbf{x}_C^{(k)} + \mathbf{y}_C$,
4. $\mathbf{x}_F^{(k+1)} = \mathbf{x}_F^{(k+1/2)} + W_{FC} \mathbf{y}_C$.

In multigrid terminology, the first step can be seen as a so-called F -relaxation step, where we approximate A_{FF}^{-1} using some simple approximation, such as with weighted Jacobi or Gauss-Seidel. The second step is a coarse-grid correction step, where the residual after F -relaxation is restricted by injection, and the coarse-grid correction, \mathbf{y}_C , is computed by solving a linear system with an approximation, \hat{A}_C , of the true Schur complement, $A_{CC} - A_{CF} A_{FF}^{-1} A_{FC}$. The final two steps correspond to an interpolation of the coarse-grid correction, writing the interpolation operator $P = \begin{bmatrix} W_{FC} \\ I \end{bmatrix}$, for some approximation of the ideal interpolation operator, $W_{FC} \approx A_{FF}^{-1} A_{FC}$. If the approximation in the first step is sufficiently poor that a significant residual is expected to remain at the F -points after relaxation, it is also reasonable to augment the restriction in the second step, using either the transpose of interpolation or some better approximation to an ideal restriction operator than just injection.

As written above, the algebraic form of reduction-based multigrid retains the key disadvantage of classical AMG — there is little connection between the algorithmic choices (of the coarse/fine partitioning, and the approximations of A_{FF} , of the Schur complement, and of the idealized interpolation and restriction operators) with the resulting convergence of the algorithm. To address these limitations, MacLachlan et al.²⁴ proposed a reduction-based AMG algorithm (AMGr) that attempts to connect convergence with properties of A_{FF} . In particular, they presented a two-level convergence theory with a convergence rate quantified by the approximation of $A_{FF} \approx D_{FF}$, with the expectation that application of D_{FF}^{-1} to both a vector and to A_{FC} is computationally feasible. In what follows, we use the standard notation that matrices $A \geq B$ when $\mathbf{x}^T A \mathbf{x} \geq \mathbf{x}^T B \mathbf{x}$ for all vectors \mathbf{x} .

Theorem 1.²⁴ Consider the symmetric and positive-definite matrix $A = \begin{bmatrix} A_{FF} & -A_{FC} \\ -A_{FC}^T & A_{CC} \end{bmatrix}$ such that $A_{FF} = D_{FF} + \mathcal{E}$, with D_{FF} symmetric, $0 \leq \mathcal{E} \leq \epsilon D_{FF}$, and $\begin{bmatrix} D_{FF} & -A_{FC} \\ -A_{FC}^T & A_{CC} \end{bmatrix} \geq 0$, for some $\epsilon \geq 0$. Define relaxation with error-propagation operator $R = (I - \sigma \begin{pmatrix} D_{FF}^{-1} & 0 \\ 0 & 0 \end{pmatrix} A)$ for $\sigma = 2/(2 + \epsilon)$, interpolation $P = \begin{bmatrix} D_{FF}^{-1} A_{FC} \\ I \end{bmatrix}$, and coarse-level correction with error-propagation operator $T = I - P(P^T A P)^{-1} P^T A$. Then the multigrid cycle with ν pre-relaxation sweeps, coarse-level correction, and ν post-relaxation sweeps has error propagation operator $\text{MG}_2 = R^\nu \cdot T \cdot R^\nu$ which satisfies

$$\|\text{MG}_2\|_A \leq \left(\frac{\epsilon}{1 + \epsilon} \left(1 + \left(\frac{\epsilon^{2\nu-1}}{(2 + \epsilon)^{2\nu}} \right) \right) \right)^{1/2} < 1. \quad (2)$$

If a partitioning and approximation, D_{FF} , of A_{FF} are found that satisfy the assumptions given above, then this theorem establishes existence of an interpolation operator, P , giving multigrid convergence with a direct tie to the approximation parameter, ϵ . In this theory, tight spectral equivalence between D_{FF} and A_{FF} is required to ensure good performance of the solver. This leads to the goal of constructing the fine-grid set so that there is a guarantee of tight spectral equivalence between D_{FF} and A_{FF} .

To meet that goal, MacLachlan and Saad¹ proposed to partition the rows and columns of the matrix A in order to ensure the diagonal dominance of A_{FF} , so that D_{FF} could be chosen as a diagonal matrix. In particular, a diagonal dominance factor is introduced for each row i , defined as

$$\theta_i = \frac{|A_{ii}|}{\sum_{j \in F} |A_{ij}|},$$

With this, A_{FF} is said to be θ -diagonally dominant if $\theta_i \geq \theta$ for all $i \in F$, where $\theta > 1/2$ measures the diagonal dominance of A_{FF} . In addition to establishing the connection between the diagonal dominance parameter θ and the convergence parameter, ϵ , MacLachlan and Saad¹ posed the partitioning algorithm as an optimization problem for given $\theta > 1/2$, asking for the largest F -set such that $\theta_i \geq \theta$ for every $i \in F$. Such a θ -dominant A_{FF} guarantees good equivalence between a diagonal matrix, D_{FF} , and A_{FF} , and the largest such F -set would make the coarse-grid problem smallest. This leads to an optimization problem of the form

$$\begin{aligned} & \max_{F \subset \Omega} |F|, \\ & \text{subject to } |A_{ii}| \geq \theta \sum_{j \in F} |A_{ij}|, \forall i \in F. \end{aligned} \quad (3)$$

The greedy algorithm¹ for (3) selects rows and columns of the matrix A for A_{FF} in a greedy manner to ensure the diagonal dominance of A_{FF} , as described in Algorithm 1. Here, the set U contains all the DoFs that are unpartitioned (not yet assigned

to be coarse or fine points). Initially, all degrees of freedom are assigned to U , while the F and C sets are empty. The rows that directly satisfy the diagonal dominance criterion are initially added to the F -set (and removed from U). If there are no diagonally dominant DoFs in the U set, then the point having the least diagonal dominance is made a C -point. This selection may make some other points in U diagonally dominant, whereupon these DoFs are added to the F -set and removed from U , and the process is repeated until the set U becomes empty.

Algorithm 1 Greedy coarsening algorithm

```

1: function GREEDY-COARSENING( $A, \theta$ )
2:    $U = \{1, 2, \dots, n\}, F = \emptyset, C = \emptyset$ 
3:    $\hat{\theta}_i = \frac{|A_{ii}|}{\sum_{j \in F \cup U} |A_{ij}|}$  for all  $i = 1, \dots, n$ 
4:   for  $i \leftarrow 1, \dots, n$  do
5:     if  $\hat{\theta}_i \geq \theta$  then
6:        $F \leftarrow F \cup \{i\}, U \leftarrow U \setminus \{i\}$ 
7:     end if
8:   end for
9:   while  $U \neq \emptyset$  do
10:     $j = \operatorname{argmin}_{i \in U} \{\hat{\theta}_i\}$ 
11:     $U \leftarrow U \setminus \{j\}, C \leftarrow C \cup \{j\}$ 
12:    for  $i \in U \cap \operatorname{Adj}(j)$  do  $\triangleright \operatorname{Adj}(j) = \{k : A_{jk} \neq 0\}$ 
13:       $\hat{\theta}_i \leftarrow \frac{|A_{ii}|}{\sum_{k \in F \cup U} |A_{ik}|}$ 
14:      if  $\hat{\theta}_i \geq \theta$  then
15:         $F \leftarrow F \cup \{i\}, U \leftarrow U \setminus \{i\}$ 
16:      end if
17:    end for
18:  end while
19:  Return  $F, C$ 
20: end function

```

3 | SIMULATED ANNEALING

The optimization problem in (3) is a combinatorial optimization problem. Because such problems arise in many areas of computational science and engineering, significant research effort has been devoted to developing algorithms for their solution, both of general-purpose type (e.g., branch and bound techniques) and for specific problems (e.g., the travelling salesman problem)²⁹. For many problems, the size of the solution space makes exhaustive brute-force algorithms infeasible; for some such problems, branch and bound techniques may be successful in paring down the solution space to a more manageable size. In many cases, however, there are no feasible exact algorithms, and stochastic search algorithms, such as simulated annealing (SA), genetic algorithms, or tabu search methods, can be employed³⁰. In this work, we apply SA algorithms to approximate the global minimum of the optimization problem in (3).

Simulated annealing (SA) is a probabilistic method used to find global optima of cost functions that might have a large number of local optima. The SA algorithm randomly generates a state at each iteration and the cost function is computed for that state. The value of the cost function for a state determines whether the state is an improvement. If the current state improves the value of the objective function, it is accepted to exploit the improved result. The current state might also be accepted, with some probability less than one, even if it is worse than the previous state, however the probability of accepting a bad state decreases exponentially with the “badness” of the state. The purpose of (sometimes) accepting inferior states, known as “exploration” is to avoid being trapped in local optima, and the inferior intermediate states are considered in order to give a pathway to a globally better solution. The total number of iterations of SA depends on an initial “temperature” and the rate of decrease of that

temperature. The temperature also affects the probability of accepting a bad state, with the exploration phase of the algorithm becoming less probable as the temperature decreases, to ensure convergence to a global optimum.

3.1 | Idea and generic algorithm

Consider the set F of fine points to be the current state. To find F that maximizes a fitness function $z(F)$, such as $z(F) = |F|$ in (3), simulated annealing proceeds as shown in Algorithm 2. The temperature T starts at an initial value and decays by a factor $\alpha \in (0, 1)$ at each iteration (the “cooling schedule”). A key choice when using simulated annealing is a method for choosing a neighbor state \tilde{F} that is close to the current state F . In the case of optimizing the choice of a subset $F \subset \Omega$, a straightforward choice is to choose \tilde{F} by randomly adding or removing an element from F . Finally, the function $P(z, \tilde{z}, T)$ is the probability of accepting a move from a current state with fitness z to the new state with fitness \tilde{z} . The standard acceptance function is

$$P(z, \tilde{z}, T) = \begin{cases} 1 & \text{if } \tilde{z} > z, \\ \exp(- (z - \tilde{z})/T) & \text{otherwise.} \end{cases} \quad (4)$$

This probability function always accepts transitions that raise the fitness, and sometimes accepts transitions that decrease the fitness. Occasionally accepting fitness-decreasing transitions is essential to escape local maxima in the energy landscape, with the chance of such transitions being controlled by the current temperature. By analogy with the physical annealing of metals, at high temperatures we will accept almost all fitness-decreasing transitions, allowing exploration of the fitness landscape, but as the temperature cools we will accept fewer of these transitions, until we eventually become trapped near a fitness maximum.

Algorithm 2 Generic simulated annealing (SA) algorithm

- 1: Initialize F to a random state and T to an initial temperature
 - 2: **for** n_{steps} iterations **do**
 - 3: Randomly pick a neighbor state \tilde{F} of F
 - 4: **if** $\text{rand}(0, 1) < P(z(F), z(\tilde{F}), T)$ **then**
 - 5: $F \leftarrow \tilde{F}$
 - 6: **end if**
 - 7: $T \leftarrow \alpha T$
 - 8: **end for**
 - 9: Return F
-

Much work has been devoted to the design of optimal transition probability functions³¹ and cooling schedules³² in simulated annealing algorithms. While it can be shown that simulated annealing converges to the global maximum with probability one as the cooling time approaches infinity³³, in practice the performance depends significantly on the selection of the neighbors \tilde{F} of the current state F . A common heuristic for choosing neighbors is to select states with similar fitness, which is more efficient because we are less likely to reject such transitions, although this is in tension with the desire to escape from steep local maxima.

There are also different algorithmic possibilities for the handling of constraints on the state F . Given a constraint subset of allowable states, one common method of enforcing the constraint is to pick only neighbor states \tilde{F} that are in the constraint subset. This method is appropriate if the constraint subset is connected and constraint-satisfying neighbors can always be found, and it is easy to see that this algorithm inherits all theoretical properties of the unconstrained version. An alternative method, which we will use in Section 3.2, is to allow constraint-violating neighbors to be selected but keep a record of the highest-fitness constraint-satisfying state visited. This method is advantageous when constraint-violating paths in state space allow rapid transitions between (possibly disconnected) areas in the constraint subset. This algorithm also preserves the global guarantees of convergence under the condition that the global maximum is constraint satisfying.

3.2 | Adaptation to coarse/fine partitioning

While it is possible to apply SA directly to the optimization problem in (3), preliminary experiments show that this is inefficient, due to the global coupling of the degrees of freedom in the optimization problem. To overcome this, we consider a domain

decomposition approach to solving the optimization problem, where we first divide the discrete set of degrees of freedom into (non-overlapping) subdomains (the construction of which is considered in detail in the following subsection) and apply SA to the subdomain problems. These subdomain problems are not independent, therefore information is exchanged about the tentative partitioning on adjacent subdomains; this is accomplished in either an additive (Jacobi-like) or multiplicative (Gauss-Seidel-like) manner. For sufficiently small subdomains, however, SA can efficiently find near-optimal solutions to localized versions of the optimization in (3), and we focus on this process below.

SA is run on each subdomain to partition its DoFs into (local) C - and F -sets. As the suitability of this partitioning in a global sense naturally depends on decisions being made on adjacent subdomains, we must be careful to consider what happens to DoFs in the global mesh adjacent to those in the subdomain. If these subdomains already have their own tentative C/F partitions computed (as is expected to be the case on all but the first sweep through the domain), then this partitioning is considered fixed, and used to guide decisions on the current subdomain. If no tentative partitioning has yet been computed on a neighbouring subdomain, then the points in the neighbouring subdomain that are connected to some DoF of the current subdomain are considered to be F -points, while all other DoFs in the neighbouring subdomain are considered to be C -points. These assumptions are used only for the purposes of computing the partitioning on the current subdomain, to apply hard constraints on the partitioning.

Specifically, if $\Omega = \{1, 2, \dots, n\}$ is the global set of degrees of freedom, partitioned into s disjoint subdomains as $\Omega = \cup_{k=1}^s \Omega_k$, then the optimization problem to be solved on subdomain k is given as

$$\begin{aligned} & \max_{F_k \subset \Omega_k} |F_k|, \\ & \text{subject to } |A_{ij}| \geq \theta \sum_{j \in F} |A_{ij}|, \forall i \in \bar{F}_k, \end{aligned}$$

where information from other subdomains enters in the constraint, both as additional points for which the constraint must be satisfied and in the right-hand side of the constraint where we sum over $j \in F$ (and not $j \in F_k$). Here, F_k is the current set of points in Ω_k that are in the F -set, and we define $C_k = \Omega_k \setminus F_k$ to be the complementary C -set. Further, we use \bar{F}_k and F to denote the sets of tentative F -points in $\bar{\Omega}_k$ and Ω , respectively, where the standard ‘‘closure’’ notation, $\bar{\Omega}_k$, denotes the set of points j , such that either $j \in \Omega_k$ or $A_{ij} \neq 0$ for some $i \in \Omega_k$. In the localized optimization problem above, the set \bar{F}_k contains both the points in F_k and any point $j \in \bar{\Omega}_k \setminus \Omega_k$ such that either j is in the F_ℓ -set in a neighbouring subdomain, Ω_ℓ , that has a tentative partition or $j \in \Omega_\ell$ for a neighbouring subdomain, Ω_ℓ that does not yet have a tentative partition.

Within an annealing step on a given subdomain, Ω_k , we take the current tentative set F_k as the initial guess for the partitioning, with the exception of the first step, where we take $F_k = \emptyset$ for all $i \in \Omega_k$ (to ensure we start from a configuration that satisfies the constraint). As a benchmark for the annealing process, we initialize $\bar{n}_F^{(k)}$ as the largest size of a constraint-satisfying F -set seen so far on Ω_k (taken to be zero on the first iteration), and z to be the number of constraint-satisfying F -points in the *current* set \bar{F}_k . At each annealing step on Ω_k , we swap points in and out of F_k , either increasing, decreasing, or maintaining its size, with equal probability. The basic algorithm for these swaps is given in Algorithm 3, where we take the sets F_k and C_k as input, along with values n_F and n_C giving the numbers of points to swap from C_k to F_k and vice-versa. We note that there are two possible ways to do this swap, either selecting the elements from F_k and C_k independently and then moving the elements, or first moving the selected elements from F_k and, then, selecting the elements from the updated set C_k to move. We follow the first way as preliminary experiments suggested that it gives slightly better results.

Algorithm 3 swapFC(F_k, C_k, n_F, n_C)

- 1: $\tilde{F}_k \leftarrow F_k$
 - 2: $\tilde{C}_k \leftarrow C_k$
 - 3: Randomly select n_C points from F_k , remove the points from \tilde{F}_k , and add the points to \tilde{C}_k
 - 4: Randomly select n_F points from C_k , remove the points from \tilde{C}_k , and add the points to \tilde{F}_k
 - 5: Return \tilde{F}_k, \tilde{C}_k
-

The main annealing step, as given in Algorithm 4, then takes the form of selecting whether to increase, decrease, or maintain the size of F_k , checking if the selected action is possible, and performing it if it is. To increase the size of F_k , we first check that C_k has sufficient entries to move. If so, we increase the size of F_k by selecting $x + y$ entries of C_k to move to F_k and y entries of F_k to move to C_k , for pre-determined values of x and y (typically $x = 1, y = 0$, although these values could also be drawn

from a suitable distribution). If the decision is made to swap points, we check that both F_k and C_k have sufficient points to swap, then swap x points from each set into the other (typically $x = 1$). Finally, if the decision is made to decrease the size of F_k , we check that it has points to remove, then move $x + y$ points from F_k to C_k and y points from C_k to F_k (ensuring $x + y > 0$; typically $x = 1, y = 0$). Finally, we measure the fitness of the resulting tentative F -set and decide whether or not to accept it before decrementing the temperature by the relative factor α and the number of further annealing steps to take by one.

Algorithm 4 Annealing on Ω_k

```

1: Initialize  $F_k$  and  $C_k$ , set  $n_{\text{steps}}, \alpha, T, \bar{n}_F^{(k)}, z$ 
2: for  $n_{\text{steps}}$  iterations do
3:   Randomly generate  $r \in \{0, 1, 2\}$  with equal probability
4:   if  $r = 0$  &  $|C_k| \geq x + y$  then
5:      $\tilde{F}_k, \tilde{C}_k = \text{swapFC}(F_k, C_k, x + y, y)$ 
6:   end if
7:   if  $r = 1$  &  $\min(|F_k|, |C_k|) > x$  then
8:      $\tilde{F}_k, \tilde{C}_k = \text{swapFC}(F_k, C_k, x, x)$ 
9:   end if
10:  if  $r = 2$  &  $|F_k| \geq x + y$  then
11:     $\tilde{F}_k, \tilde{C}_k = \text{swapFC}(F_k, C_k, y, x + y)$ 
12:  end if
13:  Construct  $\bar{F}_k, \bar{C}_k$ 
14:   $F_k, C_k, \bar{n}_F^{(k)}, z = \text{accept}(\tilde{F}_k, \tilde{C}_k, \bar{F}_k, \bar{C}_k, \bar{n}_F^{(k)}, z, T)$ 
15:   $T \leftarrow \alpha T$ 
16: end for
17: Return  $F_k, C_k$ 

```

The fitness score of a given (tentative) partition over $\bar{\Omega}_k$ is directly calculated as the number of points in the set that satisfy the diagonal dominance criterion, as outlined in Algorithm 5. In the acceptance step of the algorithm, given as Algorithm 6, we compute the fitness score for the tentative \bar{F}_k and compare it to that of the current (last accepted) set \bar{F}_k . If the fitness score increases or remains same, then we automatically accept the step and update F_k, C_k , and z . In this case, we additionally check if all points in the current \bar{F}_k -set are constraint satisfying and, if so, if this set increases the value of $\bar{n}_F^{(k)}$. If so, we update the value of $\bar{n}_F^{(k)}$ (and update the global F -set). If $\tilde{z} < z$, then the step is accepted with a probability that decreases with temperature and $z - \tilde{z}$, but the additional check need not be done.

Algorithm 5 fitness(\bar{F}_k)

```

1: Calculate diagonal dominance for each DoF in the set  $\bar{F}_k$ 
2:  $\tilde{z} \leftarrow$  the number of points that meet the diagonal dominance criterion
3: Return  $\tilde{z}$ 

```

3.3 | Localization and Gauss-Seidel variants

In Section 4, we consider both structured-grid and unstructured-grid problems; consequently, we consider both geometric and algebraic decompositions of Ω into $\{\Omega_k\}_{k=1}^s$. An important advantage of algebraic partitioning, however, is that it can be used to generate deeper multigrid hierarchies, since geometric partitioning can only be used to generate a single coarse level (which has unstructured DoF locations and, thus, does not naturally lead to further geometric partitioning). Here, we outline both strategies.

For structured grids, we can consider geometric decomposition of the fine grid into subdomains. For problems with (eliminated) Dirichlet boundary conditions, we typically satisfy the diagonal dominance criterion already at all points adjacent to a

Algorithm 6 $\text{accept}(\tilde{F}_k, \tilde{C}_k, \tilde{F}_k, \tilde{n}_f^{(k)}, z, T)$

```

1:  $\tilde{z} = \text{fitness}(\tilde{F}_k)$ 
2: if  $\tilde{z} \geq z$  then
3:    $z \leftarrow \tilde{z}, F_k \leftarrow \tilde{F}_k, C_k \leftarrow \tilde{C}_k$ 
4:   if  $\tilde{z} = |\tilde{F}_k|$  &  $\tilde{z} \geq \tilde{n}_f^{(k)}$  then
5:      $\tilde{n}_f^{(k)} \leftarrow \tilde{z}$ 
6:      $F \leftarrow (F \setminus \Omega_k) \cup \tilde{F}_k$ 
7:   end if
8: else
9:   Randomly generate  $s \in [0, 1]$ 
10:  if  $s < e^{-(z-\tilde{z})/T}$  then
11:     $z \leftarrow \tilde{z}, F_k \leftarrow \tilde{F}_k, C_k \leftarrow \tilde{C}_k$ 
12:  end if
13: end if
14: Return  $F_k, C_k, \tilde{n}_f^{(k)}, z$ 

```

Dirichlet boundary, so these points are taken as F -points from the beginning and not included in the decomposition into subdomains. A natural strategy is to subdivide the remaining points into square or rectangular subdomains of equal size (modulo boundary/corner cases). We consider this in Section 4 for both finite-difference and bilinear finite-element discretizations on uniform meshes. When the number of points (in one dimension) to be decomposed is not evenly divided by the given subdomain size (in one dimension), the right-most and bottom-most subdomains on the mesh are of smaller size, given by the remainder in that division. On structured grids, we can consider either a lexicographical Gauss-Seidel iteration over the subdomains or a four-colored Gauss-Seidel iteration. In preliminary experiments, the four-colored Gauss-Seidel iteration outperformed the lexicographical strategy, so we use this.

On both structured and unstructured grids, we also consider algebraic decomposition using Lloyd aggregation to define the subdomains. Lloyd aggregation, proposed by Bell³⁴, is a natural application of Lloyd’s algorithm³⁵ to subdivide the DoFs of a matrix into well-shaped subdomains. Given a desired number of subdomains (or average size per subdomain), the unit-distance graph of the matrix is constructed and one “center” point for each subdomain is randomly selected. Each (tentative) subdomain is then selected as the set of points that are closer to the subdomain center point than to any other subdomain center, using a modified form of the Bellman-Ford algorithm. Then, for each subdomain, the center point is reselected (again using a modified form of the Bellman-Ford algorithm), as the current centroid of the subdomain (a DoF having maximum distance from the subdomain boundary, breaking ties arbitrarily). This process is repeated (reforming subdomains around the new centers, then reassigning centers) until the assignment to subdomains has converged.

In the algebraic case, a multicoloured Gauss-Seidel iteration strategy is more complicated, since we would need to compute a colouring of the subdomains; hence, we simply use lexicographical Gauss-Seidel to iterate between subdomains.

3.4 | Benchmark results

A natural comparison is with that of the greedy strategy¹, which we provide in the following numerical results. For the structured-grid discretizations, we have also explored “hand-tuned” optimization strategies to try and maximize the size of the global F -set while satisfying the constraint.

For the five-point finite-difference stencil of the Laplacian on a uniform 2D mesh, for any value $\frac{1}{2} < \theta < \frac{4}{7}$, the diagonal dominance criterion will be satisfied if every F -point has at least one C -neighbour. An optimal strategy³⁶ for this case arises by dividing the fine mesh into “X-pentominos”, sets of five grid points with one center point and its four cardinal neighbours, plus edge/corner cases where only a subset of an X-pentomino is needed. Then, the C -set can be selected as the center points of each X-pentomino (or subset of one), with the remaining points assigned to the F -set. In an ideal case (e.g., with periodic boundary conditions, or minimal edge cases), this leads to an F -set with size equal to $4/5$ of the size of Ω . Such a coarsening is shown in the left panel of Figure 1. Note that some points adjacent to Dirichlet BCs are naturally chosen as coarse points in this strategy, despite their inherent diagonal dominance, because they are center points of an X-pentomino that includes just one point in

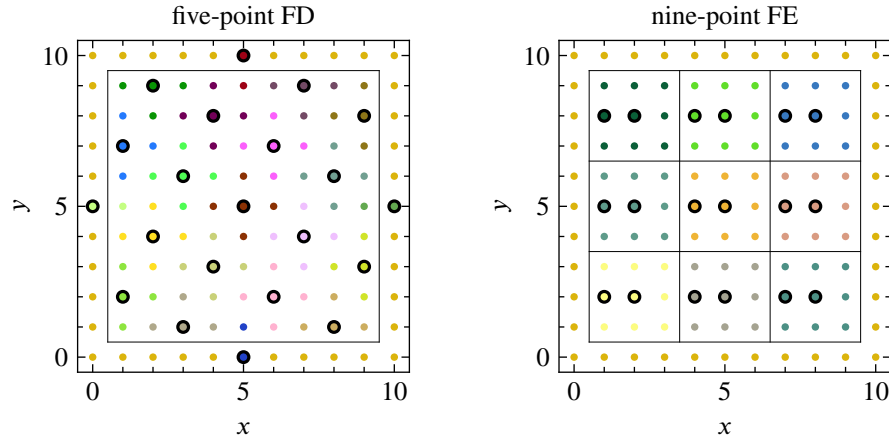


FIGURE 1 Splitting of C - and F - points for 11×11 meshes from “by-hand” optimization. At left, X-pentomino coarsening for five-point FD scheme. At right, 3×3 brick coarsening for nine-point FE scheme. At left, we color by the X-pentominos and at right, we color by the 3×3 bricks. C -points are represented by the black circles.

the region away from the boundary. These could be equally well treated by making the interior point in these X-pentominos a C -point and leaving the center point on the boundary as an F -point, but there is no advantage to doing so.

For the nine-point bilinear finite-element discretization of the Laplacian on a uniform 2D mesh, for any value of θ less than $4/7$, the diagonal dominance criterion will be satisfied if every F -point has at least two C -neighbours. Here, we partition the points (again except those adjacent to a Dirichlet boundary) into square subdomains of size 3×3 , and select two points consistently in each subdomain as C -points. In an ideal case, where we can fill the domain with 3×3 “bricks”, this leads to an F -set with $7/9$ of the size of Ω . Such a coarsening is shown in the right panel of Figure 1. When the domain cannot be filled perfectly with 3×3 bricks, the remaining square/rectangular regions still require one or two C points to be selected, reducing the optimal size of the resulting F set.

4 | RESULTS

In the results below, we set the initial (global) temperature at $T = 1$, and compute the reduction rate, α , so that $\alpha^{n_{ts}} = 0.1$, where n_{ts} is the total number of annealing steps to be attempted. Thus, all experiments end when the global temperature reaches 0.1. In addition, for each problem, we determine n_{ts} by fixing a total number of steps per DoF in the system, and report results based on the allotted number of steps per DoF. This work is further subdivided into Gauss-Seidel sweeps by fixing values of the number of annealing steps per DoF per sweep, with the number of sweeps determined as the ratio of total steps per DoF to steps per DoF per sweep.

We first consider structured-grid experiments for both the finite-difference (five-point) and bilinear finite element (nine-point) discretizations of the Laplacian, using a 32×32 mesh to explore how much work is needed to determine near-optimal partitions using both geometric and algebraic divisions into subdomains. Using these experiments to identify “best practices”, we then explore how the coarsening algorithm performs as we change the problem size, move from structured to unstructured finite-element meshes, and isotropic to anisotropic operators.

4.1 | Structured-grid discretizations with geometrically structured subdomains

We start by considering the five-point finite-difference stencil on a fixed (uniform) 32×32 mesh, and consider the effects of changing both the size of the Gauss-Seidel subdomains and the distribution of work in the algorithm. As a measure of quality of the results, we consider the maximum of the ratio $|F|/|\Omega|$ over all constraint-satisfying F -sets generated in a single run of the annealing algorithm. As a comparison, for this problem, the best “by-hand” optimization of the size of the F -set yields $|F|/|\Omega| = 0.8047$, as depicted by the blue lines in Figure 2, while the greedy algorithm¹ yields $|F|/|\Omega| = 0.561$ (not depicted because it is far from the data shown here). We vary three algorithmic parameters in Figure 2, the total number of SA steps per

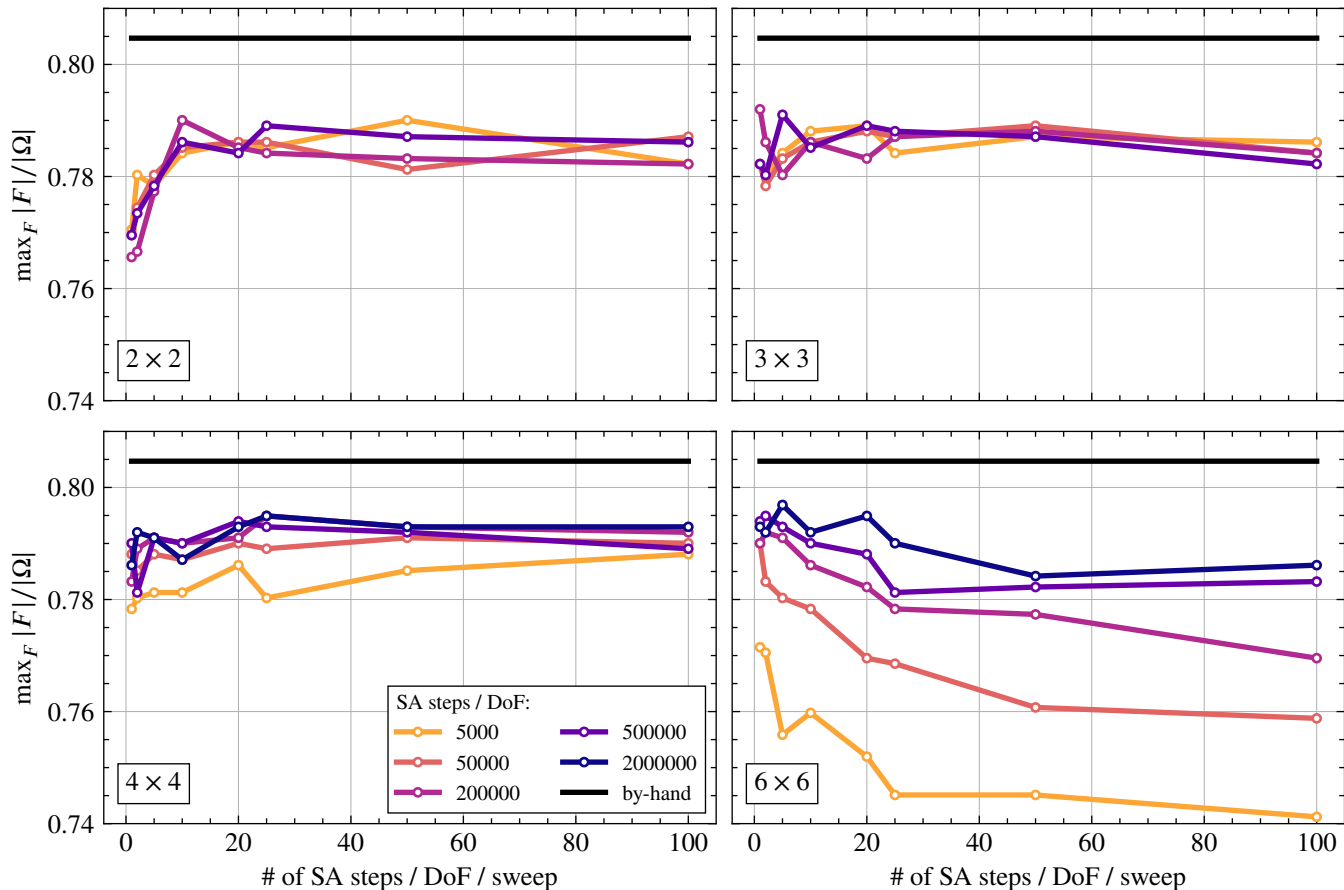


FIGURE 2 Maximum value of $|F|/|\Omega|$ with number of annealing steps per DoF per GS sweep for different numbers of annealing steps per DoF for the 32×32 uniform-grid five-point finite-difference discretization. Each panel shows a different size of geometrically chosen subdomain: 2×2 (top-left), 3×3 (top-right), 4×4 (bottom-left), 6×6 (bottom-right).

DoF, with values ranging from 5000 to 2 000 000, the number of SA steps per DoF in a single sweep of Gauss-Seidel on each subdomain, and the size of the subdomains used in the Gauss-Seidel sweeps. Of these, the number of SA steps per DoF per sweep of Gauss-Seidel is correlated least with the quality of results. For the smallest subdomain sizes (in particular, the 2×2 subdomains at the top left of Figure 2), we see a sharp improvement in performance when increasing this parameter from 1 to about 10, but plateauing results beyond that. For larger subdomains, there is again some advantage in most cases to choosing a value slightly larger than 1, but little advantage in choosing large values (and, indeed, we see sharp degradation in performance with larger values of this parameter on the 6×6 mesh at bottom right). Thus, in further results, we generally fix this value to be relatively small, either 1 or 5.

For small subdomain sizes — e.g., the 2×2 and 3×3 subdomain cases shown in the top row of Figure 2 — we observe little benefit of increasing the total amount of work in the algorithm, with comparable results for all numbers of total annealing steps per DoF. In contrast, for the 6×6 subdomains (bottom right of Figure 2), we see strong stratification of the results with increasing total number of SA steps. The 4×4 case also shows improving behaviour with increasing number of total SA steps, albeit less-so than with larger subdomains. Overall, we see this consistently in our numerical results: for small subdomain sizes, the quality of coarsening achieved quickly stagnates, with each subdomain having too little freedom to make adjustments into better global configurations while still satisfying local constraints. For larger subdomains, we see both better overall configurations and improvements with larger work budgets; however, we also see increasing numbers of SA steps per DoF needed to achieve the best performance.

A key question is how to balance the parameters in the SA algorithm to achieve reasonable performance at an acceptable cost. To examine this, we fix the total number of annealing steps per DoF and consider the best partitioning achieved by varying the

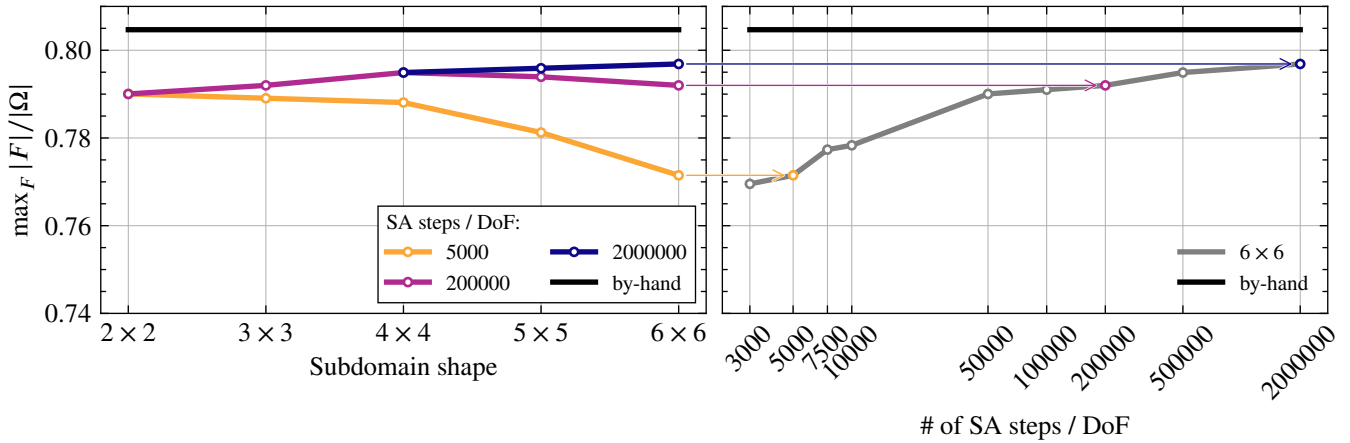


FIGURE 3 Left: Change in $|F|/|\Omega|$ with subdomain size for the 32×32 uniform-grid five-point finite-difference discretization, using geometric subdomains, with 5000, 200 000, and 2 000 000 total SA steps per DoF. Right: Change in maximum number of F -points with number of total SA steps per DoF for this problem using 6×6 subdomains.

subdomain size in the left panel of Figure 3. Here, we run for a number of different values of the number of SA steps per DoF per Gauss-Seidel sweep, and take the best partitioning observed over these grids for each subdomain size (noting that the optimal choice varies somewhat with subdomain size, typically being larger for small subdomain sizes and smaller for large subdomain sizes). When using 200 000 SA steps per DoF, there is a clear maximum in the graph for 4×4 subdomains, although the relative difference in quality is not substantial; however, when using 2 000 000 SA steps per DoF, we see continued improvement in the quality of the partitioning up to the 6×6 subdomain case. In the right panel of Figure 3, we look more closely at the convergence of the results with increasing numbers of SA steps per DoF for the case of 6×6 subdomains, again taking the best results obtained for different values of the number of SA steps per DoF per Gauss-Seidel sweep. Here, we see a clear improvement in the results up to $\mathcal{O}(10^5)$ SA steps per DoF, and continued improvement up to 2 000 000 SA steps per DoF.

A natural question that arises from the right-hand panel of Figure 3 is whether the best meshes obtained occur early or late in the annealing process. That is, while we clearly see benefit from slow “cooling” of the annealing process (many SA steps per DoF), it is important to identify *when* the optimal results are obtained during the annealing process. Figure 4 shows the annealing history for a sample run, on the 32×32 uniform grid five-point finite-difference stencil, with 2 000 000 SA steps per DoF (for a total of almost 2×10^9 annealing steps). At right, we see the temperature decay, following an exponential curve from $T = 1.0$ at the first step to $T = 0.1$ at the final step. At left, we plot the changes in the ratio $|F|/|\Omega|$ compared to the by-hand optimal mesh for this grid (also shown). For comparison, the ratio from the greedy algorithm is also shown. We see that after an initial rapid improvement in the value of the ratio, there is a secondary period where performance improves notably but steadily, up to between 5×10^8 and 10^9 total annealing steps. This demonstrates that many annealing steps are, indeed, needed to reach the best partitioning seen here, although a good partitioning is still found after many fewer steps.

We next address the nature of the grids generated by annealing, and whether they resemble grids that could be selected geometrically for this problem. Figure 5 shows two of the grids generated, along with the subdomains used in their generation. These represent the “best” grids found by the annealing procedure, with ratios of $|F|/|\Omega|$ of around 0.795. While these grids yield competitive ratios, there is no clear global geometric pattern, nor obvious relationship to the best by-hand optimized grid shown in Figure 1. Furthermore, there are no clear improvements of these grids that could be readily made, such as single coarse points that could be omitted without leading to constraint violations. This suggests that the energy landscape for this problem is likely dominated by locally optimal configurations that are separated by states with constraint violations and/or sharp changes in energy.

Figure 6 shows how the performance of the annealing algorithm scales with problem size, for both the geometric choice of subdomains for the finite-difference discretization discussed so far, and for the finite-element discretization. In addition, an algebraic selection (discussed below) is added for comparison. All methods (including the by-hand optimization) perform relatively well for small meshes, but degrade as the mesh size increases. The amount of work needed to achieve these results with the annealing algorithm also increases with grid size. For the 8×8 mesh, using a single (global) subdomain, equally-good partitions to the by-hand optimization can be found with just 2000 annealing steps per DoF (and fewer when more subdomains

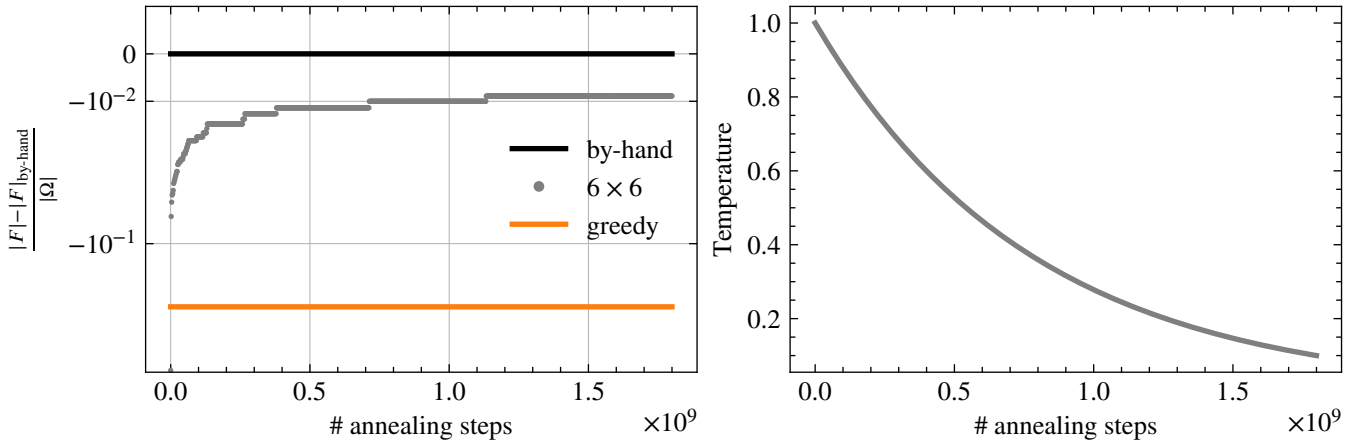


FIGURE 4 Change in $|F|/|\Omega|$ (left) and temperature (right) with number of annealing steps for the 32×32 uniform-grid finite-difference discretization of the Laplacian. At left, the case of SA with five SA steps per DoF per GS sweep using 6×6 subdomain size is shown, along with greedy as a baseline. Note that the vertical axis on the left plot uses a mixed log-linear scale for clarity, with a break at -10^{-2} .

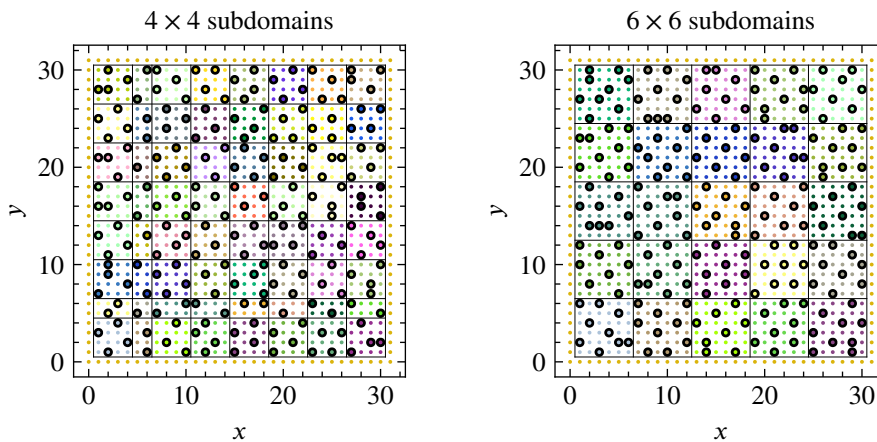


FIGURE 5 Grid partitioning for 32×32 uniform grid with five-point FD stencil using two million SA steps per DoF. At left, the partitioning is generated using primarily 4×4 subdomains, with 25 SA steps per DoF per cycle. At right, the partitioning is generated using 6×6 subdomains, with 5 SA steps per DoF per cycle. The grid at left has 814 F -points, while that at right has 816.

are used). For the 16×16 mesh, more work and larger subdomains are needed to achieve such performance. With small (2×2 or 3×3) subdomains, even using 200 000 annealing steps per DoF did not achieve performance equal to the by-hand partitioning on the 16×16 mesh. For larger subdomains, the algorithm did equal the results of the by-hand partitioning, but with increasing work as subdomain size increased: for 4×4 subdomains, 10 000 annealing steps per DoF are needed, while 50 000 annealing steps per DoF are needed for 5×5 subdomains. For 6×6 subdomains, even using 200 000 annealing steps per DoF, we could not recover results matching the by-hand partitioning, although we speculate that this would have occurred with even more work invested. For larger domain sizes, the results shown in Figure 6 represent the best results found for a given grid over all runs with varying subdomain sizes, total SA steps per DoF, and SA steps per DoF per GS sweep.

For the nine-point finite-element (FE) stencil, we see similar results to those reported above and, consequently, do not include figures detailing the individual experiments in as much detail. Most notably, the best partitioning that we achieve by hand is a slightly worse in this case (as detailed in Section 3.4), and the partitioning using the greedy algorithm is better than in the FD case, yielding $|F|/|\Omega| = 0.752$. At left of Figure 7, we show an analogous figure to Figure 2 for the case of 5×5 subdomains.

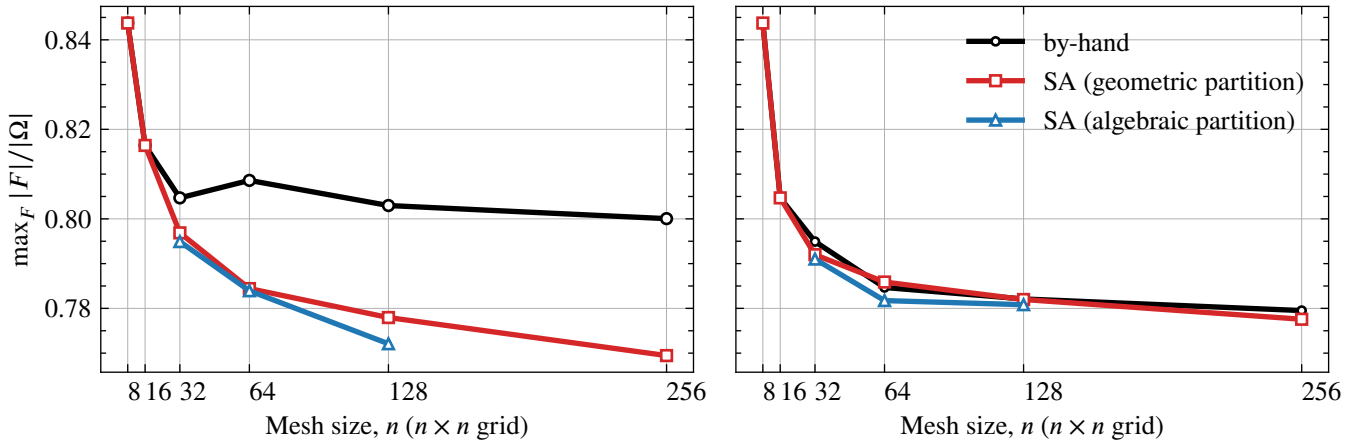


FIGURE 6 Change in $|F|/|\Omega|$ with mesh size for FD (left) and FE (right) discretizations.

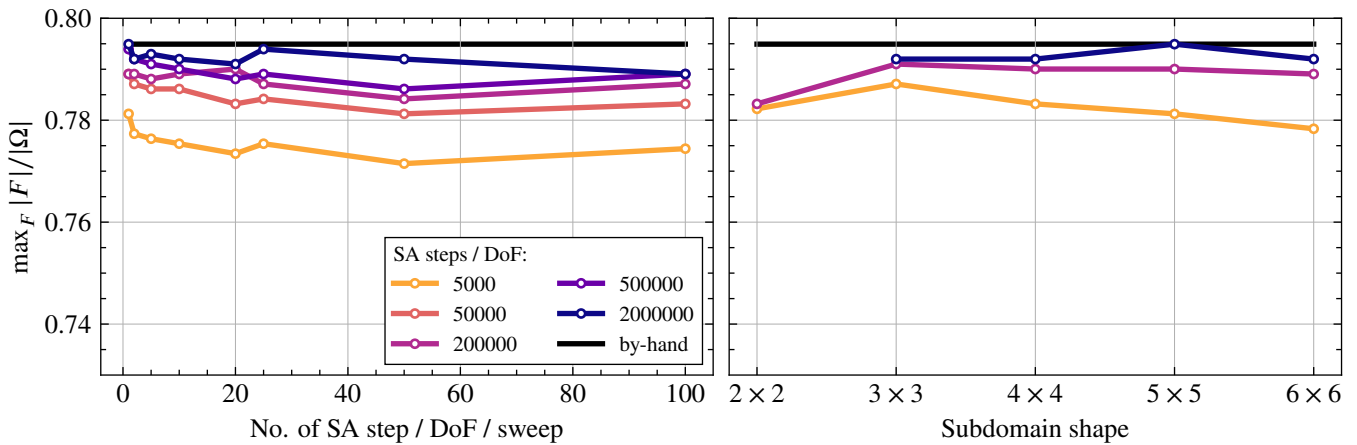


FIGURE 7 Quality of coarsening for the 32×32 uniform-grid nine-point finite-element discretization, using geometric subdomains. Left: Maximum value of $|F|/|\Omega|$ with number of annealing steps per DoF per GS sweep for different numbers of annealing steps per DoF using 5×5 geometric subdomains. Right: Change in $|F|/|\Omega|$ with subdomain size and total number of SA steps per DoF.

Here, we observe the same stratification. However, we are able to recover the same quality of partitioning as the best by-hand partitioning using 5×5 subdomains and 2 000 000 SA steps per DoF. Also note that we see the same mild dependence on the number of SA steps per DoF per sweep as we did in the FD case. The right panel of Figure 7 shows how the quality of partitioning changes with subdomain size and total work budget. Similarly, there is an improvement in performance with additional work for larger subdomain sizes, but that improvement stagnates with additional work for smaller subdomain sizes. Sample grids generated for the finite-element case, including colouring to indicate subdomain choice, are shown in Figure 8.

Finally, we verify that the result two-level AMGr algorithms are at least as effective as predicted in theory, by measuring asymptotic convergence factors (ρ), grid complexities (C_{grid} , equal to the ratio of sum of the number of DoFs on each level of the hierarchy to that on the finest level), and operator complexities (C_{op} , equal to the ratio of the sum of the number of nonzero entries in the system matrix on each level of the hierarchy to that on the finest level). We approximate ρ by running the cycle with a random initial guess, $x^{(0)}$, and zero right-hand side, and then compute $(\|x^{(k)}\| / \|x^{(0)}\|)^{1/k}$, where $x^{(k)}$ is the approximation (to the true solution, which is the zero vector) after k cycles. Because the convergence factors of AMGr are somewhat larger than those for classical AMG, we take $k = 800$ to ensure that we sample the asymptotic behaviour suitably. Table 1 reports this data for two-level cycles for both the FD and FE discretizations, for both the geometric subdomain choice considered here and the algebraic subdomain choice discussed next. Considering the geometric subdomain choice, we see that the convergence

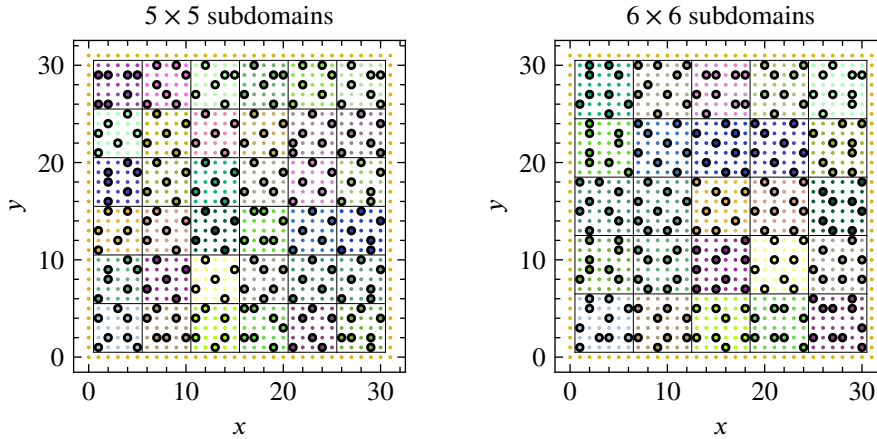


FIGURE 8 Grid partitioning for 32×32 uniform grid with nine-point FE stencil using two million SA steps per DoF. At left, the partitioning is generated using 5×5 subdomains, with one SA step per DoF per cycle. At right, the partitioning is generated using 6×6 subdomains, also with one SA step per DoF per cycle. The grid at left has 814 F -points, while that at right has 811.

TABLE 1 Performance of two-level AMGr on test matrices from discretizations of the 2D Laplacian.

Scheme	Grid size	Geometric Subdomains			Algebraic Subdomains		
		ρ	C_{grid}	C_{op}	ρ	C_{grid}	C_{op}
FD	8×8	0.85	1.16	1.12	0.85	1.16	1.12
	16×16	0.86	1.19	1.18	0.86	1.19	1.18
	32×32	0.88	1.20	1.20	0.88	1.20	1.20
	64×64	0.89	1.22	1.22	0.89	1.22	1.22
	128×128	0.89	1.22	1.23	0.89	1.22	1.23
FE	8×8	0.70	1.16	1.15	0.70	1.16	1.15
	16×16	0.63	1.20	1.22	0.63	1.20	1.22
	32×32	0.67	1.21	1.23	0.69	1.21	1.25
	64×64	0.71	1.21	1.25	0.72	1.22	1.27
	128×128	0.71	1.22	1.27	0.71	1.22	1.27

factors are better than the theoretical upper bound of 0.977, and relatively consistent for each discretization. Notably, neither the convergence factor nor the measured complexities degrade substantially with problem size.

4.2 | Structured-grid discretizations with algebraically chosen subdomains

We next consider partitioning the structured-grid problems using an algebraic choice of the subdomains based on Lloyd aggregation. Figure 9 shows the change in the maximum number of F -points (scaled by the total number of DoFs) with the change of the subdomain size for both the FD and FE discretizations (left and right, respectively). Similarly to the case of geometric partitioning, we see relatively poor performance for small subdomain sizes, regardless of the work allocated to the SA process. For larger subdomain sizes, we see improving results with number of SA steps per DoF, as seen above. Also as seen above, the optimal subdomain size varies with total work allocation, increasing as we increase the amount of work per DoF, but even with 2 000 000 SA steps per DoF, we do not see the best performance with largest subdomains for the FE discretization. Considering variation in problem size, Figure 6 shows that, as in the geometric subdomain case, we see some decrease in performance as problem size grows, but that this decrease seems to (mostly) plateau at larger problem sizes. In comparison with the geometric subdomain choice, we see some small degradation in performance with algebraically chosen subdomains, particularly in the FD case, but it is small in comparison with the optimality gap between the by-hand optimized solutions and those generated by SA.

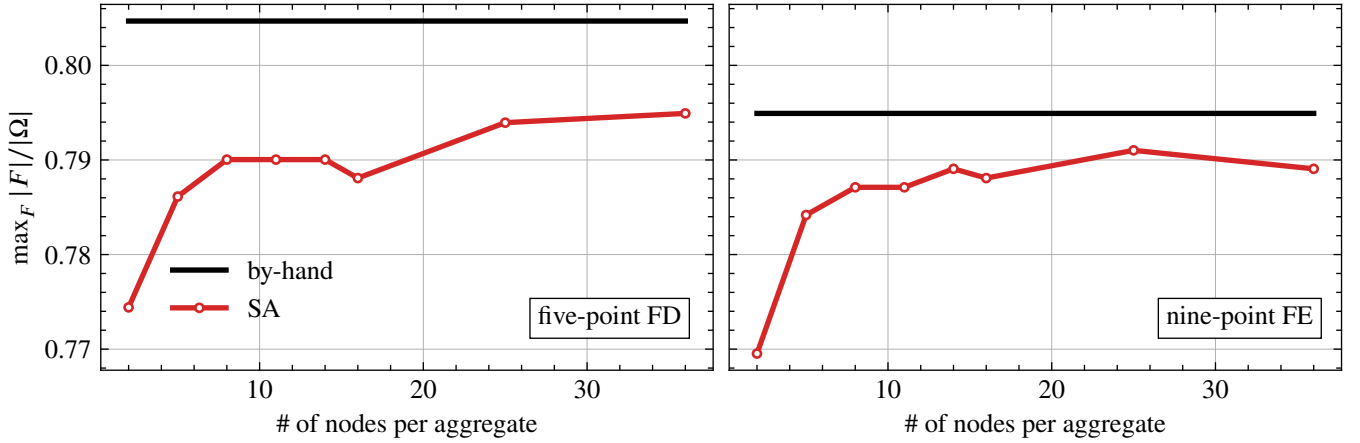


FIGURE 9 Change in maximum number of F -points with subdomain size for algebraic subdomain selection on 32×32 meshes. Left and right figures are for FD and FE schemes, respectively, showing the largest value of $|F|/|\Omega|$ attained over experiments with fixed subdomain size and varying the total number of SA steps per DoF and SA steps per sweep, as in the geometric subdomain case.

TABLE 2 Performance of three-level AMGr on test matrices from discretizations of the 2D Laplacian.

Scheme	Grid size	Three-level V-cycle			Three-level W-cycle		
		ρ	C_{grid}	C_{op}	ρ	C_{grid}	C_{op}
FD	32×32	0.78	1.25	1.31	0.68	1.25	1.31
	64×64	0.92	1.27	1.28	0.88	1.27	1.28
	128×128	0.92	1.28	1.30	0.88	1.28	1.30
FE	32×32	0.78	1.25	1.31	0.68	1.25	1.31
	64×64	0.77	1.27	1.35	0.71	1.27	1.35
	128×128	0.80	1.28	1.37	0.70	1.28	1.37

Performance of the resulting two-grid cycles is tabulated in Table 1, where we see very comparable convergence factors, as well as grid and operator complexities, as in the geometric subdomain case. Table 2 tabulates convergence factors, grid complexities, and operator complexities for three-level V- and W-cycles. For the FD case, we see some degradation in convergence when using V-cycles, while W-cycles give convergence factors similar to those in the two-level case. For the FE problem, there is less degradation for V-cycles, but still W-cycles are required to get convergence factors comparable to the two-level case. As we have increased the depth of the multigrid hierarchy, the grid and operator complexities in Table 2 are naturally larger than those in Table 1, but the growth in these complexity measures is consistent with optimally scaling multigrid methods.

4.3 | Anisotropic problems on structured grids

Next, we consider the two-dimensional anisotropic diffusion problem, $-\nabla \cdot \mathbf{K}(x, y) \nabla u(x, y) = f(x, y)$ in the domain $[0, 1] \times [0, 1]$ with Dirichlet boundary conditions. We choose the tensor coefficient $\mathbf{K}(x, y) = \mathbf{Q} \mathbf{M} \mathbf{Q}^T$, where $\mathbf{Q} = \begin{bmatrix} \cos(\theta) & -\sin(\theta) \\ \sin(\theta) & \cos(\theta) \end{bmatrix}$, and

$\mathbf{M} = \begin{bmatrix} \delta & 0 \\ 0 & 1 \end{bmatrix}$. The parameters $0 < \delta \leq 1$ and θ specify the strength and direction of anisotropy in the problem, respectively, with $\theta = 0$ giving the anisotropic problem $-\delta u_{xx} - u_{yy} = f$ and $\theta = \pi/2$ giving $-u_{xx} - \delta u_{yy} = f$. For $0 < \theta < \pi/2$, the axis of the small diffusion coefficient in the problem rotates clockwise from being in the positive x -direction for small θ to the positive y -direction for $\theta \approx \pi/2$. Anisotropic problems cause difficulty for the greedy coarsening algorithm¹, where large grid and

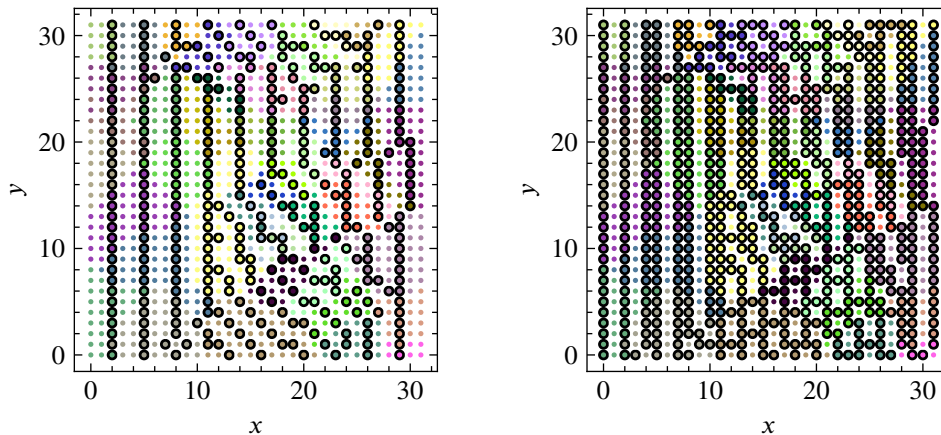


FIGURE 10 Grid partitioning for an anisotropic diffusion problem with $\delta = 10^{-6}$ and $\theta = \pi/3$, discretized on a 32×32 mesh using the bilinear FE stencil. The initial partitioning, at left, is generated using algebraic subdomains averaging 20 points per subdomain, using 2 000 000 SA steps per DoF and 1 SA step per DoF per GS sweep, and has 664 F -points and 360 C -points. At right is the grid augmented using the second pass of the classical AMG algorithm, resulting in 343 F -points and 681 C -points.

operator complexities and poor algorithmic performance were overcome by augmenting the coarse grids with the second pass of the Ruge-Stüben coarsening algorithm and using classical AMG interpolation in place of the AMGr interpolation operator.

As an example of a problem in this class, we fix $\delta = 10^{-6}$ and $\theta = \pi/3$. Figure 10 shows the coarse-grid points selected for the bilinear finite-element discretization of the problem on a uniform 32×32 mesh. At left, we see that the partitioning generated by the SA algorithm correctly detects that this is an anisotropic problem with strong coupling primarily in the x -direction and weak coupling primarily in the y -direction, producing grids that are consistent with semi-coarsening, with some regions of coarsening along diagonals. Unfortunately, however, this grid leads to poor convergence using AMGr interpolation. As in the original experiments by MacLachlan and Saad¹, each fine-grid point has multiple coarse-grid neighbours (leading to an increase in operator complexity, due to the nonzero structure of $D_{FF}^{-1}A_{FC}$), but since A is no longer diagonally dominant in the anisotropic case, the assumption that $\begin{bmatrix} D_{FF} & -A_{FC} \\ -A_{FC}^T & A_{CC} \end{bmatrix}$ is positive semi-definite is violated, and the resulting performance is poor. To overcome this failure, we augment the coarse-grid set using the second-pass algorithm from Ruge-Stüben AMG, using the classical strength of connection parameter of 0.30 to determine strong connections in the graph. At right of Figure 10, we show the resulting graph, which now satisfies the requirement that every pair of strongly connected F -points has a common C -neighbour (which is clearly not satisfied in the partitioning at left). Unfortunately, this comes at a heavy cost, as the grid at right now has many more C -points than we would like. Below, we verify that these grids lead to effective multigrid hierarchies, when coupled with classical AMG interpolation, but note the increased grid and operator complexities in these hierarchies. A key question for future work is whether we can determine algebraic interpolation operators for grids such as those at left that lead to effective AMGr performance.

Tables 3 and 4 present convergence factors and grid and operator complexities for two- and three-level cycles, respectively. For geometric partitioning, we use 200 000 SA steps per DoF with one or two SA steps per DoF per cycle and 5×5 or 6×6 subdomains (depending on what worked best for a given problem). Similar choices are made using algebraic partitioning, although we see slight improvements using 2 000 000 SA steps per DoF for some problems. For the three-level tests, we uniformly use 200 000 SA steps per DoF, with 1 SA step per DoF per GS sweep, and algebraic subdomains with average size of 36 points. In Table 3, we again see that there is relatively little difference in results generated using geometric and algebraic choices of the Gauss-Seidel subdomains. Notably, both choices lead to effective cycles for both the finite-difference and finite-element discretizations, albeit at the cost of increased grid and operator complexities. Table 4 again shows degradation in performance moving from two-grid to three-grid V-cycles, but that three-grid W-cycles mostly recover comparable convergence to the two-level case, with some notable degradation for the finite-element operator.

TABLE 3 Performance of two-level AMGr for the anisotropic diffusion problem with $\delta = 10^{-6}$ and $\theta = \pi/3$ on structured meshes.

Scheme	Grid size	Geometric Partitioning			Algebraic Partitioning		
		ρ	C_{grid}	C_{op}	ρ	C_{grid}	C_{op}
FD	32×32	0.58	1.70	2.09	0.57	1.70	2.09
	64×64	0.58	1.71	2.11	0.58	1.71	2.11
	128×128	0.60	1.72	2.12	0.63	1.72	2.12
FE	32×32	0.62	1.65	2.02	0.61	1.67	2.00
	64×64	0.61	1.67	2.09	0.62	1.67	2.08
	128×128	0.61	1.67	2.11	0.61	1.67	2.12

TABLE 4 Performance of three-level AMGr for the anisotropic diffusion problem with $\delta = 10^{-6}$ and $\theta = \pi/3$ on structured meshes.

Scheme	Grid size	Three-level V-cycle			Three-level W-cycle		
		ρ	C_{grid}	C_{op}	ρ	C_{grid}	C_{op}
FD	32×32	0.72	2.16	3.13	0.57	2.16	3.13
	64×64	0.76	2.16	3.20	0.60	2.16	3.20
	128×128	0.80	2.18	3.26	0.66	2.18	3.26
FE	32×32	0.74	2.06	2.86	0.61	2.06	2.86
	64×64	0.81	2.07	3.05	0.69	2.07	3.05
	128×128	0.89	2.05	3.10	0.82	2.05	3.10

4.4 | Discretizations on unstructured grids

For our final tests, we consider two diffusion problems with homogeneous Dirichlet boundary conditions on unstructured triangulations of square domains, discretized using linear finite elements. First, we consider an isotropic diffusion operator ($-\nabla \cdot \nabla u = f$) on $[-1, 1]^2$, generated by taking an initially unstructured mesh, refining it a set number of times, and then smoothing the resulting mesh. We consider three levels of refinement for this example, resulting in meshes with 1433, 5617, and 22 241 DoFs. The SA-based partitioning scheme appears to perform similarly well in this setting, with a splitting found for the smallest mesh shown in Figure 11. While we no longer have hand-generated estimates of the optimal coarsening factors, we note that the SA-based partitioning scheme outperforms the greedy algorithm, generating F -sets with 1106, 4241, and 16 604 points, for these three grids, respectively, in comparison to F -sets of 1024, 3916, and 15 079 points. Two- and three-level convergence factors, as well as grid and operator complexities for these systems are given in Table 5. Here, we observe that these results are quite similar to those seen for the structured-grid discretizations above, with some degradation in convergence seen for the three-level V-cycle results, but not in the W-cycle results. Here, the three-level results are computed using 200 000 SA steps per DoF, with 1 SA step per DoF per GS sweep, on subdomains with an average of 36 points per subdomain. Slight modifications to these parameters yield small improvements in two-level results; as a result, we use these choices in the table.

We next consider the anisotropic diffusion operator (again with Dirichlet boundary conditions) considered above, with $\delta = 0.01$ and $\theta = \pi/3$, on an unstructured triangulation of the unit square taken from Brannick and Falgout²³, matching the problem labelled 2D-M2-RLap in that paper. As in Brannick and Falgout²³, we consider three levels of refinement of the mesh, with 798, 3109, and 12 273 DoFs, respectively. Figure 12 shows two different partitions for this mesh. At left, we give the partitioning generated using the SA-based partitioning algorithm proposed here, and at right we give the splitting after a second pass of the Ruge-Stüben coarsening algorithm where strength of connection is computed using the classical strength parameter of 0.55. As with the structured-grid case above, we found the second pass is needed to achieve good convergence factors for the anisotropic problem, but that it does so at the expense of coarsening at a much slower rate. Convergence factors, grid complexities, and operator complexities for these problems are reported in Table 6. As above, the complexities are higher for the

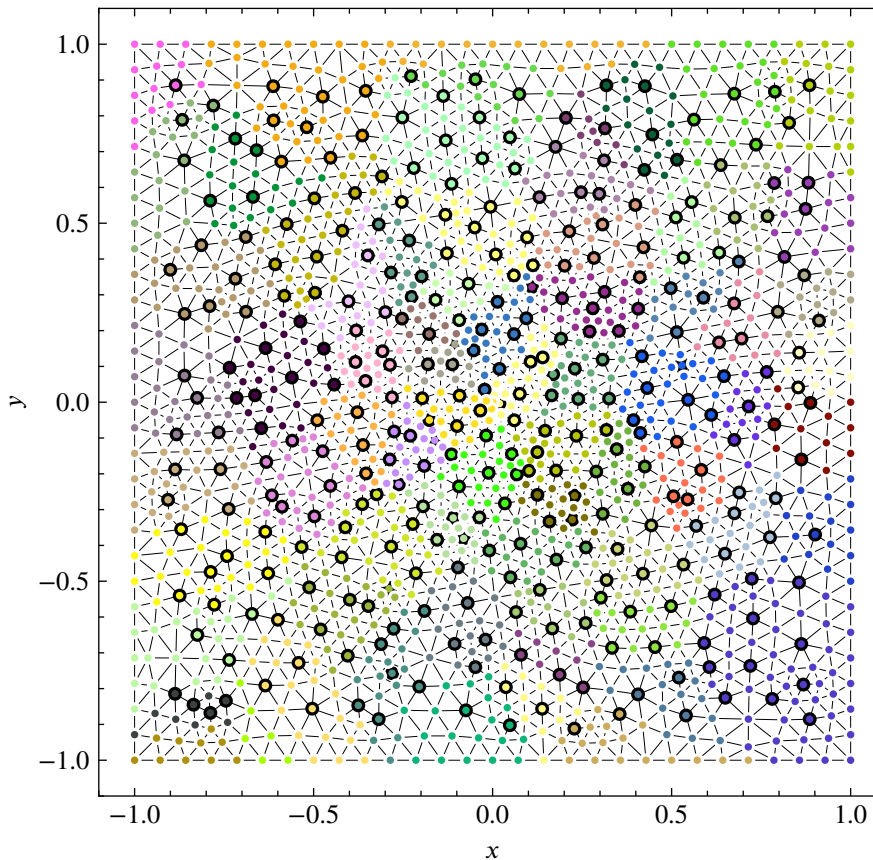


FIGURE 11 Partitioning for the isotropic problem on the unstructured mesh with 1433 points, generated using 1 000 000 SA steps per DoF, 5 SA steps per DoF per GS sweep, and subdomains with an average of 20 points per subdomain.

TABLE 5 Performance of two- and three-level AMGr for isotropic problem on unstructured meshes.

#DoF	Two-level V-cycle			Three-level V-cycle			Three-level W-cycle		
	ρ	C_{grid}	C_{op}	ρ	C_{grid}	C_{op}	ρ	C_{grid}	C_{op}
1433	0.66	1.23	1.31	0.78	1.28	1.39	0.65	1.28	1.39
5617	0.71	1.25	1.32	0.79	1.30	1.42	0.70	1.30	1.42
22241	0.75	1.25	1.33	0.84	1.32	1.45	0.75	1.32	1.45

anisotropic operators than the isotropic (due to the use of the second pass). Here, we observe degradation in convergence with grid refinement, although again with less degradation for W-cycles than V-cycles. The three-level results are computed with the same parameters as for the isotropic problem above, with more SA steps per DoF used for the two-level results, as this yielded slight improvements. While the performance reported in Table 6 is far from optimal, we note that the convergence factors for the larger two meshes are better than those reported for compatible relaxation²³, while the operator complexities are comparable to those reported therein for BoomerAMG⁵.

5 | CONCLUSIONS AND FUTURE WORK

In this paper, we propose a new coarsening algorithm for AMGr, based on applying simulated annealing to the optimization problem first posed by MacLachlan and Saad¹. For isotropic problems on both structured and unstructured meshes, we find that

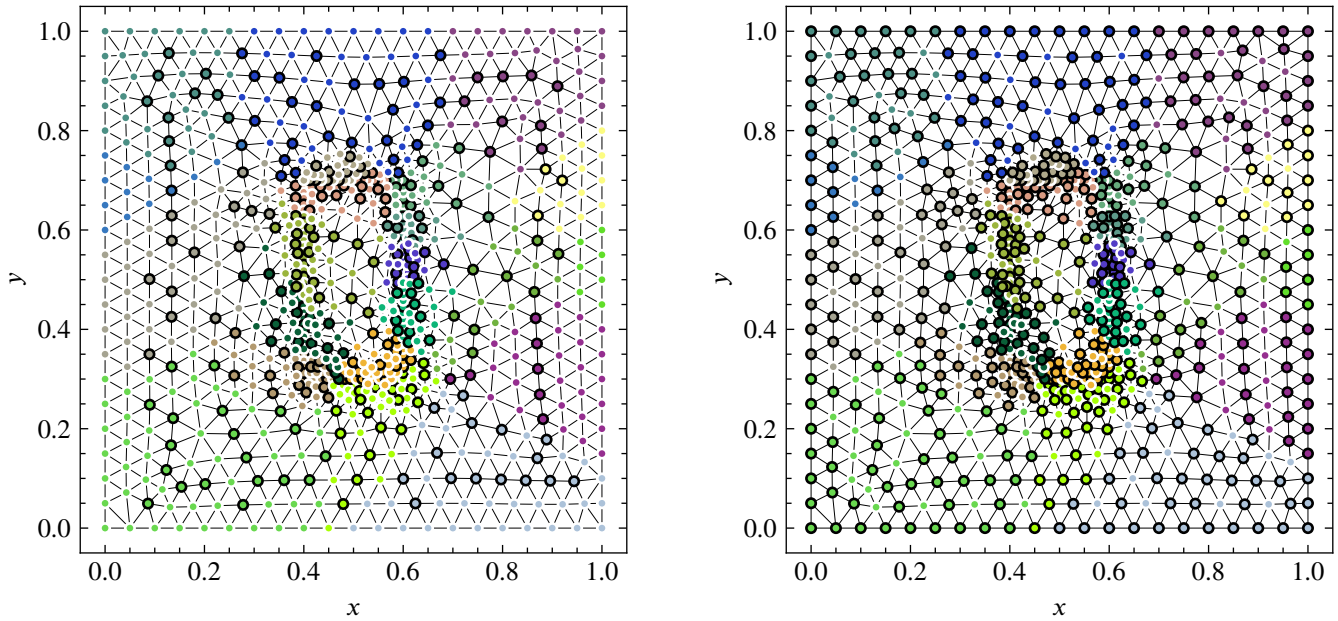


FIGURE 12 Partitioning for the anisotropic problem on an unstructured mesh containing 798 points. The partitioning at left was generated using 500 000 SA steps per DoF, with 1 SA step per DoF per GS sweep, on subdomains with an average size of 36 points per subdomain, yielding 524 F -points and 274 C -points. At right, this partitioning is augmented by the second pass of classical AMG coarsening, resulting in 263 F -points and 535 C -points.

TABLE 6 Performance of two-level and three-level AMGr for anisotropic problem on unstructured meshes.

#DoF	Two-level V-cycle			Three-level V-cycle			Three-level W-cycle		
	ρ	C_{grid}	C_{op}	ρ	C_{grid}	C_{op}	ρ	C_{grid}	C_{op}
798	0.69	1.67	1.82	0.84	2.11	2.41	0.71	2.11	2.41
3109	0.75	1.67	1.87	0.84	2.09	2.52	0.75	2.09	2.52
12273	0.82	1.67	1.89	0.90	2.08	2.56	0.83	2.08	2.56

the SA-based partitioning approach outperforms the original greedy algorithm, sometimes dramatically, while sharing some of the existing limitations of the AMGr framework, particularly for anisotropic problems. Nonetheless, we see this as an important proof-of-concept, showing that randomized search and other derivative-free optimization algorithms can be successfully applied to the combinatorial optimization problems in AMG coarsening.

The main drawback of this approach is the high computational cost of simulated annealing. For example, computing a single coarse grid for a 32×32 mesh with 200 000 SA steps per DoF required around 2.5 hours on a modern workstation, primarily for evaluating the fitness functional in the optimization, with expected scaling in problem size and number of SA steps per DoF. Two key questions that this raises are whether the fitness functional can be approximated in a more efficient manner (e.g., using a value neural network) and whether other optimization techniques that rely on fewer samplings of the fitness functional can be applied. Both of these are topics of our current research.

This research also exposes a known weakness of the AMGr methodology (and, to our knowledge, one of all AMG-like algorithms with guarantees on convergence rates) when applied to problems that are not diagonally dominant (such as finite-element discretizations of anisotropic diffusion equations). Another current research direction is identifying whether the diagonal choice of D_{FF} can be generalized to yield better convergence (while retaining a guaranteed convergence rate), and whether such changes can be accommodated within the optimization problems solved here.

ACKNOWLEDGMENTS

The work of S.P.M. was partially supported by an NSERC Discovery Grant. This work does not have any conflicts of interest.

References

1. MacLachlan S, and Saad Y. A greedy strategy for coarse-grid selection. *SIAM Journal on Scientific Computing*. 2007;**29**(5):1825–1853.
2. Brandt A, McCormick SF, and Ruge JW. 1982. *Algebraic multigrid (AMG) for automatic multigrid solutions with application to geodetic computations*. Inst. for Computational Studies, Fort Collins, Colo.
3. Brandt A, McCormick SF, and Ruge JW. Algebraic multigrid (AMG) for sparse matrix equations. In: Evans DJ, editor. *Sparsity and Its Applications*. Cambridge: Cambridge University Press; 1984. p. 257–284.
4. Falgout RD, and Yang UM. hypre: a Library of High Performance Preconditioners. In: *Computational Science - ICCS 2002: International Conference, Amsterdam, The Netherlands, April 21-24, 2002. Proceedings, Part III*. vol. 2331 of *Lecture Notes in Computer Science*. Springer-Verlag; 2002. p. 632–641.
5. Henson VE, and Yang UM. BoomerAMG: a Parallel Algebraic Multigrid Solver and Preconditioner. *Applied Numerical Mathematics*. 2002;**41**:155–177.
6. Balay S, Buschelman K, Eijkhout V, Gropp WD, Kaushik D, Knepley MG, et al.. 2008. *PETSc Users Manual*. ANL-95/11 - Revision 3.0.0. Argonne National Laboratory.
7. Balay S, Buschelman K, Gropp WD, Kaushik D, Knepley MG, McInnes LC, et al.. 2010. *PETSc Web page*. [Http://www.mcs.anl.gov/petsc](http://www.mcs.anl.gov/petsc).
8. Heroux MA, Bartlett RA, Howle VE, Hoekstra RJ, Hu JJ, Kolda TG, et al. An overview of the Trilinos project. *ACM Trans Math Softw*. 2005;**31**(3):397–423.
9. Gee MW, Siefert CM, Hu JJ, Tuminaro RS, and Sala MG. 2006. *ML 5.0 Smoothed Aggregation User's Guide*. SAND2006-2649. Sandia National Laboratories.
10. Olson LN, and Schroder JB. 2018. *PyAMG: Algebraic Multigrid Solvers in Python v4.0*. Release 4.0. Available from: <https://github.com/pyamg/pyamg>.
11. Vaněk P, Mandel J, and Brezina M. Algebraic multigrid by smoothed aggregation for second and fourth order elliptic problems. *Computing*. 1996;**56**(3):179–196.
12. Stüben K. An introduction to algebraic multigrid. In: Trottenberg U, Oosterlee C, and Schüller A, editors. *Multigrid*. London: Academic Press; 2001. p. 413–528.
13. Ruge JW, and Stüben K. Algebraic multigrid (AMG). In: McCormick SF, editor. *Multigrid Methods*. vol. 3 of *Frontiers in Applied Mathematics*. Philadelphia, PA: SIAM; 1987. p. 73–130.
14. Alber DM, and Olson LN. Parallel coarse-grid selection. *Numerical Linear Algebra with Applications*. 2007;**14**(8):611–643. Available from: <http://dx.doi.org/10.1002/nla.541>.
15. Cleary AJ, Falgout RD, Henson VE, and Jones JE. Coarse-Grid Selection for Parallel Algebraic Multigrid. In: *Proc. of the Fifth International Symposium on Solving Irregularly Structured Problems in Parallel*. vol. 1457 of *Lecture Notes in Computer Science*. New York: Springer-Verlag; 1998. p. 104–115.
16. De Sterck H, Yang UM, and Heys JJ. Reducing complexity in parallel algebraic multigrid preconditioners. *SIAM J Matrix Anal Appl*. 2006;**27**(4):1019–1039.

17. De Sterck H, Falgout RD, Nolting JW, and Yang UM. Distance-two interpolation for parallel algebraic multigrid. *Numer Linear Algebra Appl.* 2008;**15**(2-3):115–139.
18. Olson LN, Schroder JB, and Tuminaro RS. A new perspective on strength measures in algebraic multigrid. *Numerical Linear Algebra with Applications.* 2010 August;**17**(4):713–733. Available from: <http://dx.doi.org/10.1002/nla.669>.
19. Brannick J, Brezina M, MacLachlan S, Manteuffel T, McCormick S, and Ruge J. An energy-based AMG coarsening strategy. *Numer Linear Alg Appl.* 2006;**13**:133–148.
20. Chow E. An Unstructured Multigrid Method Based on Geometric Smoothness. *Numer Linear Alg Apps.* 2003;**10**:401–421.
21. Bröker O. Parallel Multigrid Methods using Sparse Approximate Inverses (Ph.D. Thesis). Swiss Federal Institute of Technology, Zurich. Zurich, Switzerland; 2003.
22. Livne O. Coarsening by compatible relaxation. *Numer Linear Alg Appl.* 2004;**11**(2):205–227.
23. Brannick JJ, and Falgout RD. Compatible Relaxation and Coarsening in Algebraic Multigrid. *SIAM Journal on Scientific Computing.* 2010;**32**(3):1393–1416.
24. MacLachlan S, Manteuffel T, and McCormick S. Adaptive reduction-based AMG. *Numer Linear Alg Appl.* 2006;**13**:599–620.
25. MacLachlan S, and Saad Y. Greedy coarsening strategies for nonsymmetric problems. *SIAM J Sci Comput.* 2007;**29**(5):2115–2143.
26. Gossler F, and Nabben R. On AMG methods with F-smoothing based on Chebyshev polynomials and their relation to AMGr. *Electron Trans Numer Anal.* 2016;**45**:146–159.
27. Ries M, Trottenberg U, and Winter G. A note on MGR methods. *J Lin Alg Applic.* 1983;**49**:1–26.
28. Swarztrauber PN. The methods of cyclic reduction, Fourier analysis and the FACR algorithm for the discrete solution of Poisson’s equation on a rectangle. *SIAM Rev.* 1977;**19**(3):490–501.
29. Korte B, and Vygen J. *Combinatorial Optimization: Theory and Algorithms.* 6th ed. Springer; 2018.
30. Schneider J, and Kirkpatrick S. *Stochastic Optimization.* Springer; 2006.
31. Franz A, Hoffmann KH, and Salamon P. Best Possible Strategy for Finding Ground States. *Phys Rev Lett.* 2001;**86**:5219–5222.
32. de Vicente J, Lanchares J, and Hermida R. Placement by thermodynamic simulated annealing. *Physics Letters A.* 2003;**317**(5):415–423.
33. Granville V, Krivanek M, and Rasson JP. Simulated annealing: A proof of convergence. *IEEE Transactions on Pattern Analysis and Machine Intelligence.* 1994;**16**(6):652–656.
34. Bell W. Algebraic multigrid for discrete differential forms (Ph.D. Thesis). University of Illinois at Urbana-Champaign; 2008.
35. Lloyd S. Least squares quantization in PCM. *IEEE transactions on information theory.* 1982;**28**(2):129–137.
36. Taghibakhshi A, MacLachlan S, Olson L, and West M. 2021. *Optimization-Based Algebraic Multigrid Coarsening Using Reinforcement Learning.* arXiv preprint arXiv:2106.01854.

How to cite this article: T. U. Zaman, S. P. MacLachlan, L. N. Olson, and M. West (2021), Coarse-Grid Selection Using Simulated Annealing, *Numerical Linear Algebra with Applications, Volume 1*.